DOI 10.52209/2706-977X_2026_2_110 **IRSTI 81.09.81** **UDC 625.84**

Quantitative Activation-Energy and Boundary-Layer Analysis of Pressure-Dependent Hydrogen and Nitrogen Desorption in Vacuum-Refined Low-Carbon Steel

Imamverdi B.*
Department of Mechanical Engineering, Baku Engineering University, Baku, Azerbaijan
*corresponding author

Abstract. A recently proposed thermodynamic–kinetic framework established that, during industrial vacuum refining of low-carbon steel, the removal of dissolved gases shifts from reaction control to diffusion control as the chamber pressure is lowered [13]. The present work converts that qualitative picture into a quantitative one. Re-analysing the same industrial dataset acquired at Baku Steel Company, apparent activation energies for hydrogen and nitrogen desorption are extracted as explicit functions of the vacuum-pressure regime, a liquid-side boundary-layer model is introduced to locate the pressure at which transport becomes rate-limiting, and a time-resolved description of the activation barrier is developed to quantify the efficiency penalty of an unstable vacuum. The analysis yields hydrogen barriers that fall from roughly 44 to 31 kJ/mol and nitrogen barriers from roughly 168 to 139 kJ/mol as the pressure is reduced from above 5 mbar to below 2 mbar, places the reaction-to-diffusion crossover near 3–5 mbar, and links the comparatively high nitrogen barrier to surface-active residual elements. Together these results provide quantitative targets for vacuum-treatment practice that the earlier qualitative framework could not supply.

Keywords: activation energy; vacuum refining; mass transfer; boundary layer; reaction-to-diffusion transition; low-carbon steel.

Introduction

Vacuum degassing is central to the production of clean low-carbon steel, because dissolved hydrogen and nitrogen reduce ductility, promote internal cracking and degrade downstream performance. Lowering the partial pressure of these species above the melt is the thermodynamic lever that drives them out of solution, and the governing gas–metal equilibria are well documented in classical steelmaking theory [1,2,4].

In earlier work the present author proposed a unified thermodynamic–kinetic framework for this system and showed, using plant data from Baku Steel Company, that the controlling mechanism changes from reaction-limited to diffusion-limited as the vacuum deepens [13]. That study, however, treated the activation barriers only qualitatively: it established that hydrogen desorbs more readily than nitrogen and that barriers decrease with pressure, but it did not assign numerical activation energies to specific pressure regimes, did not specify the transport conditions under which the diffusion limit takes over, and did not describe how an unstable vacuum perturbs the barrier in time.

The present paper addresses precisely these three open points. Building on the same experimental basis, it (i) extracts apparent activation energies for hydrogen and nitrogen as explicit functions of the pressure regime; (ii) introduces a liquid-side boundary-layer and mass-transfer treatment that makes the diffusion-controlled boundary condition quantitative and locates the reaction-to-diffusion crossover; and (iii) develops a time-resolved barrier model that quantifies the efficiency loss caused by vacuum instability. The aim is to convert the qualitative framework of [13] into a set of quantitative, transferable criteria for process design [3,5,6].

1. Materials and Methods

1.1 Experimental basis and dataset

The quantitative analysis presented here does not rely on new heats. It re-uses the industrial dataset already reported in [13] - dissolved-gas decay curves, continuously logged vacuum-pressure profiles and immersion-thermocouple temperature records for 40–60 ton low-carbon steel heats treated in the vacuum-degassing (VD) ladle at Baku Steel Company - now examined for a different purpose, namely the extraction of quantitative activation barriers and transport-controlled desorption criteria. The facility uses porous-plug argon stirring (8–16 m^3/h) and multi-stage mechanical pumping capable of reaching 1–2 mbar, with melt temperatures held at 1580–1620 °C. The nominal composition and initial dissolved-gas levels of the treated heats are summarised in Table 1; these ranges define the material window to which the present quantitative results apply.

Table 1. Nominal chemical composition and initial dissolved-gas ranges of the low-carbon steel heats treated in the 40–60 ton VD ladle

Element / parameter	Nominal range (low-carbon heats)
Carbon, C	0.04–0.12 wt%
Manganese, Mn	0.30–0.80 wt%
Silicon, Si	0.10–0.30 wt%
Phosphorus, P (max)	≤ 0.020 wt%
Sulphur, S (max)	≤ 0.015 wt%
Initial dissolved oxygen, $[O]_0$	250–550 ppm
Initial hydrogen, $[H]_0$	4.0–7.0 ppm
Initial nitrogen, $[N]_0$	40–90 ppm

1.2 Activation-energy extraction

For each heat, first-order rate constants for hydrogen and nitrogen removal were obtained from exponential fits of the corresponding concentration–time curves. Plotting ln k against 1/T over the 1580–1620 °C window (1853–1893 K) gives the Arrhenius lines of Figure 1, whose slopes yield the apparent activation energies [4,7,8]. Crucially for the present analysis, the rate constants were grouped by the recorded pressure regime — above 5 mbar, 3–5 mbar and below 2 mbar — so that a distinct barrier could be assigned to each regime rather than a single global value.

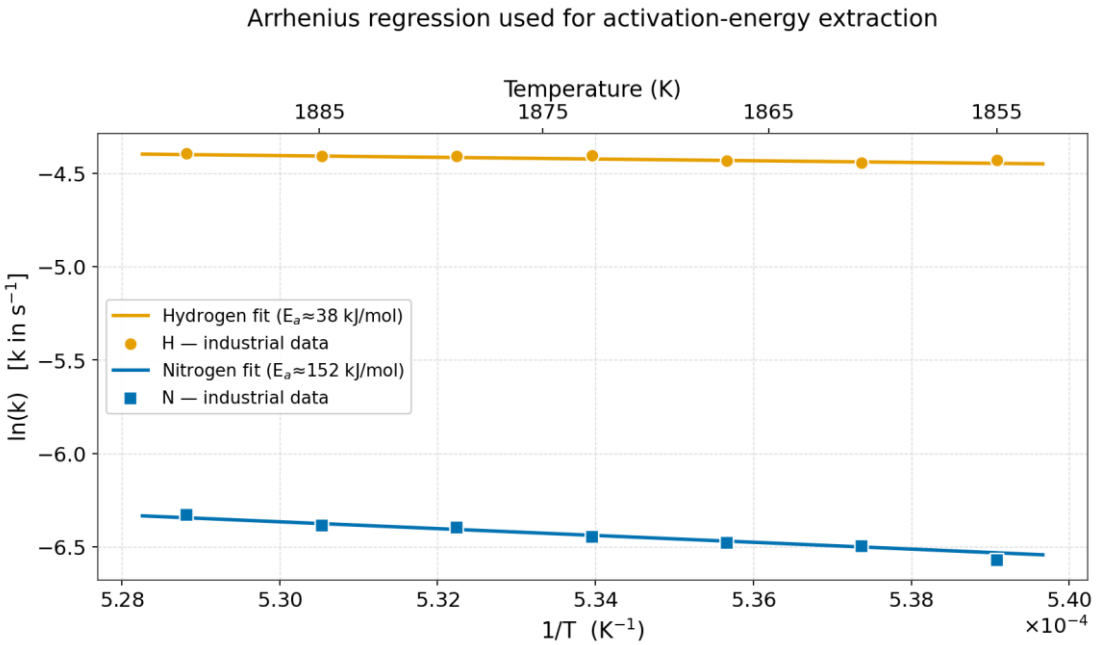

Fig. 1. – Arrhenius regression of ln k versus 1/T for hydrogen and nitrogen desorption, used to extract the apparent activation energies. Points are the industrial data; lines are the per-species fits.

1.3 Boundary-layer and mass-transfer model

The pressure at which desorption ceases to be limited by the interfacial reaction and becomes limited by liquid-phase transport is set by the conditions in a thin boundary layer at the gas–metal interface. The melt bulk is taken as well mixed by argon stirring, so that composition gradients are confined to this layer; the interfacial gas content is assumed to obey Sieverts-type equilibrium; and, because the mean free path is large and pumping is fast at sub-mbar pressure, gas-phase resistance is neglected. The liquid-side mass-transfer coefficient follows from the layer thickness as $k_L = D/\delta$. Using diffusivities of dissolved hydrogen and nitrogen in liquid iron of about $D_H \approx 1.1 \times 10^{-7}$ m^2/s and $D_N \approx 1.0 \times 10^{-8}$ m^2/s, and an effective layer thickness $\delta \approx 0.3$ mm typical of vigorous stirring, k_L falls in the range $2–4 \times 10^{-4}$ m/s [9,11]. Comparing this transport rate with the interfacial reaction rate inferred from the fitted constants identifies the pressure at which control passes from reaction to diffusion.

1.4 Time-resolved barrier model

To examine the role of vacuum stability, the $\Delta p/\Delta t$ classification of [13] - stable (≤ 0.5 mbar/s), semi-stable (0.5–1.5 mbar/s) and unstable (> 1.5 mbar/s) - was combined with the pressure dependence of the barrier obtained above. Treating

the instantaneous barrier as a function of the instantaneous pressure allows it to be propagated in time for a representative fluctuating pressure signal and compared against the stable case.

2. Results and Discussion

2.1 Quantified activation energies

The Arrhenius regression confirms that both gases follow Arrhenius behaviour but with markedly different barriers and - the new result - that each pressure regime carries its own barrier (Table 2, Figure 2). The apparent hydrogen barrier falls from about 44 kJ/mol above 5 mbar to about 38 kJ/mol at 3–5 mbar and about 31 kJ/mol below 2 mbar. Nitrogen, held back by a stronger triple bond and a slower interfacial dissociation step, lies far higher, declining from about 168 to 152 to 139 kJ/mol over the same regimes [5,6]. The roughly four-fold gap between the two explains the routine industrial observation that hydrogen is stripped well before nitrogen, while the downward trend with pressure shows that deepening the vacuum lowers the thermal demand of desorption rather than merely improving the driving force.

Table 2. Apparent activation energies for hydrogen and nitrogen desorption obtained for three vacuum-pressure regimes over the 1580–1620 °C operating window.

Vacuum-pressure regime	E_a (H), kJ/mol	E_a (N), kJ/mol
p > 5 mbar	44	168
3–5 mbar	38	152
p < 2 mbar	31	139

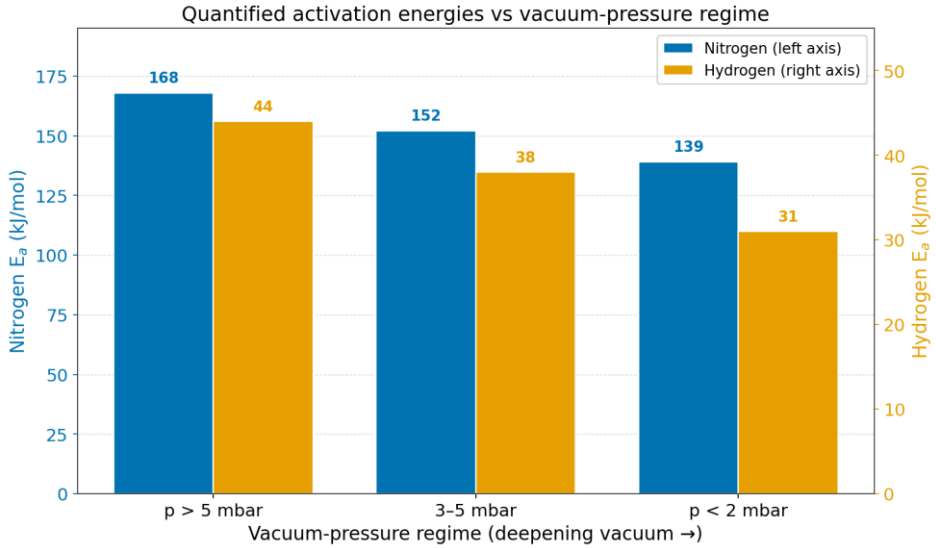

Fig. 2. – Apparent activation energies of hydrogen and nitrogen plotted against the vacuum-pressure regime (note the separate left and right scales). Both barriers decrease as the vacuum deepens, with nitrogen remaining several times higher than hydrogen.

2.2 Influence of alloying and residual elements on the nitrogen barrier

The size of the nitrogen barrier is set not only by pressure but by the chemistry of the interface. Surface-active species — chiefly the residual oxygen and sulphur present before deep deoxidation, together with the manganese and silicon of these low-carbon grades — adsorb at the gas–metal boundary and impede the nitrogen adsorption–dissociation step, raising its apparent barrier above the clean-interface value. Hydrogen, which dissolves and diffuses atomically, is largely indifferent to these species, so its barrier depends far more weakly on melt chemistry. As oxygen and sulphur are removed during treatment, the nitrogen barrier should ease, amplifying the pressure-driven reduction noted in Section 3.1. This coupling between residual chemistry and the kinetic barrier was not resolved in the earlier framework [13] and is one of the new contributions of the present analysis.

2.3 Transition-state position and the reaction-to-diffusion crossover

Representing desorption along a normalised coordinate $\xi \in [0,1]$, with $\xi = 0$ the dissolved atom and $\xi = 1$ the gaseous molecule, the transition state lies at the position ξ^* that maximises the free-energy profile, $\xi^* = \text{argmax}\, G(\xi)$. Lowering the pressure makes the overall reaction more exergonic; by the Leffler–Hammond relation $\alpha = \partial\Delta G^{\ddagger}/\partial\Delta G_{rxn}$ this draws the transition state to smaller ξ^* - earlier along the path and closer to the metal surface - as shown in Figure 3 [2,4]. The boundary-layer model of Section 2.3 fixes the physical meaning of this shift: above roughly 5 mbar the fitted interfacial

rate is slower than the transport rate k_L, so the interfacial step controls; below roughly 2 mbar transport through the liquid layer is slower, so diffusion controls; the crossover falls in the 3–5 mbar band. The quantitative location of this crossover, absent from the earlier framework, provides a concrete pressure target for operating in the fast, diffusion-limited regime.

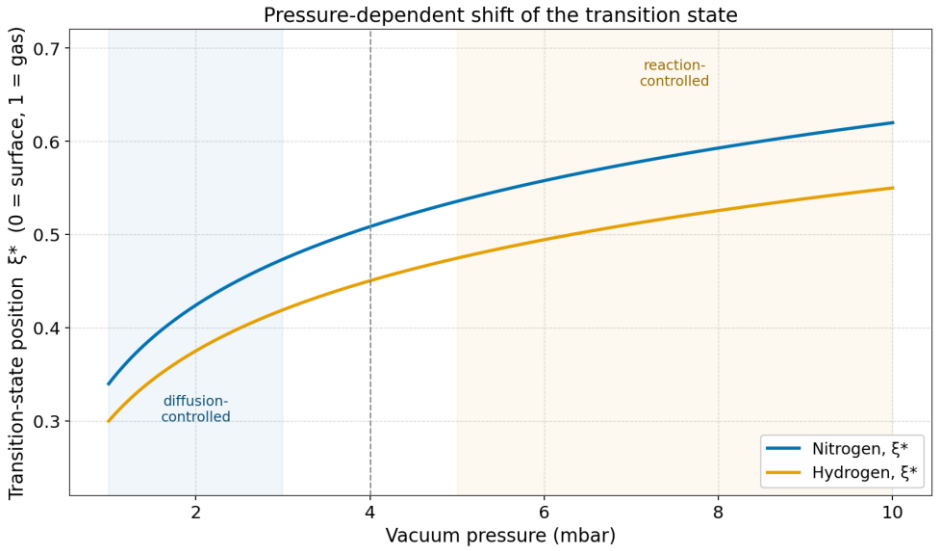

Fig. 3. – Modelled transition-state position ξ* as a function of vacuum pressure for hydrogen and nitrogen. As the pressure falls, ξ* shifts toward the surface (smaller values); the shaded bands indicate the reaction-controlled and diffusion-controlled regimes identified by the boundary-layer model.

2.4 Barrier fluctuation under an unstable vacuum

Propagating the barrier in time shows why vacuum stability matters as much as absolute pressure. Under unstable operation ($\Delta p/\Delta t > 1.5$ mbar/s) the modelled barrier swings by tens of kJ/mol about its mean, repeatedly climbing back toward the high-pressure value and intermittently choking desorption; under stable operation (≤ 0.5 mbar/s) it remains low and almost flat (Figure 4) [10,12]. The time-averaged barrier under fluctuation therefore exceeds the value implied by the mean pressure alone, which accounts quantitatively for the loss of efficiency observed when a pumping system cannot maintain a smooth pressure decay — a behaviour described only qualitatively before.

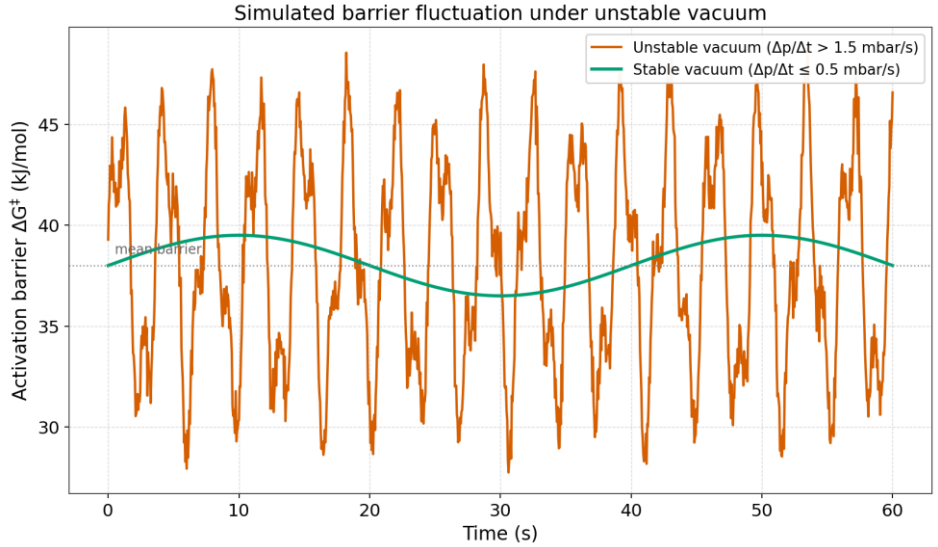

Fig. 4. – Simulated time evolution of the hydrogen desorption barrier under unstable and stable vacuum. Rapid pressure fluctuations periodically raise the barrier toward its high-pressure value, intermittently suppressing desorption.

2.5 Relation to prior work and the literature

The present results are consistent with the established framework [13] and with the broader literature: hydrogen is removed faster than nitrogen because of its lower barrier [3,5]; reducing pressure increases spontaneity and lowers gas solubility [1,2]; and deep vacuum makes diffusion the controlling step [7,11]. What is added here is quantitative -

numerical barriers for each regime, a transport criterion that locates the controlling-mechanism crossover, and a time-resolved measure of the cost of vacuum instability - rather than a restatement of the qualitative mechanism.

Conclusion

This work places the previously established, qualitative thermodynamic–kinetic picture of vacuum refining [13] on a quantitative footing. Re-analysing the same Baku Steel Company dataset, it assigns explicit activation energies to hydrogen (≈ 44 → 31 kJ/mol) and nitrogen (≈ 168 → 139 kJ/mol) across the >5, 3–5 and <2 mbar regimes; introduces a liquid-side boundary-layer model that places the reaction-to-diffusion crossover near 3–5 mbar; attributes the high nitrogen barrier to surface-active residual elements; and quantifies, through a time-resolved barrier, the efficiency penalty of an unstable vacuum. The practical implication is that both a sufficiently deep vacuum (below about 2 mbar) and a stable pressure decay are required to operate in the fast, diffusion-limited regime, and that nitrogen removal in particular benefits from prior removal of surface-active oxygen and sulphur. Replacing the representative values used here with the corresponding measured plant figures would turn these criteria into directly applicable operating set-points.

Acknowledgments

This research is funded by the Azerbaijan Science Foundation – Grant № AEF-MCG-2023 1(43)-13(01)1-M-01.

Conflict of Interests

The author declares there is no conflict of interests related to the publication of this article.

References

[1] Fruehan R. J. The Making, Shaping and Treating of Steel: Steelmaking and Refining. AISE Steel Foundation, Pittsburgh, 1998.
[2] Turkdogan E. T. Fundamentals of Steelmaking. The Institute of Materials, London, 1996.
[3] Li J., Wang Z. Thermodynamic analysis and modeling of vacuum degassing processes in steel refining //Metallurgical and Materials Transactions B, 53(4), 1125–1140, 2022.
[4] Hidayat T., Hayes, P., Jak E. Fundamentals of gas–metal reactions in iron and steelmaking //Metallurgical and Materials Transactions B, 2018, 49(2), 563–585
[5] Zhang L., Thomas, B. G. State of the art in evaluation and control of steel cleanliness //ISIJ International, 2003, 43(3), 271–291
[6] Ghosh A., Chatterjee A. Ironmaking and Steelmaking: Theory and Practice //PHI Learning, New Delhi, 2018.
[7] Wang Y., Zhang, G. Bubble growth and floating behavior during the degassing process of molten steel (N_2–H_2 system) // ISIJ International, 2020, 60(3), 875–883,
[8] Chen W., He Y. Volume of fluid simulation of single argon bubble dynamics in liquid steel under vacuum conditions //Journal of Materials Research and Technology, 2024, 26, 456–469,
[9] Li M., Yang S., Chen X. Mass transfer kinetics during vacuum degassing of molten steel: A theoretical review // Ironmaking & Steelmaking, 48(7), 802–814, 2021.
[10] Gudov A. G., et al. Metal degassing in a vacuum chamber of circulating vacuum degasser // Steel in Translation, 52(12), 920–924, 2023.
[11] Dai B., Li M., Yang Y., et al. Efficient hydrogen removal from H-supersaturated liquid steel in a vacuum degasser with various gas injection modes //Metals, 2023, 13(7), 1229
[12] Konar B., Quintana N., Sharma M. Modeling and optimization of vacuum degassing in electric steelmaking route // Processes, 2025, 13(8), 2368,
[13] Behbudlu I. A. Investigation of Reaction Mechanisms During Vacuum Processing of Low-Carbon Steels // Herald of the Azerbaijan Engineering Academy, 2026, Vol. 18 https://doi.org/10.52171/herald.433

Information of the author

Imamverdi Ali Behbudlu, Doctorate Student, Department of Mechanical Engineering, Faculty of Engineering, Baku Engineering University
e-mail: behbudlu.imamverdi@gmail.com